Title
Ternary polymer nanocomposites with concurrently enhanced dielectric constant and breakdown strength for high-temperature electrostatic capacitors

Journal
InfoMat, 2(2)

ISSN
2567-3165

Authors
Li, H
Ren, L
Ai, D
et al.

Publication Date
2020-03-01

DOI
10.1002/inf2.12043

Peer reviewed

Received: 16 July 2019 | Revised: 18 August 2019 | Accepted: 28 August 2019

DOI: 10.1002/inf2.12043

ORIGINAL ARTICLE

WILEY

Ternary polymer nanocomposites with concurrently enhanced dielectric constant and breakdown strength for high-temperature electrostatic capacitors

He Li[1,2] | Lulu Ren[1,3] | Ding Ai[1,4] | Zhubing Han[1] | Yang Liu[1] | Bin Yao[1] | Qing Wang[1]

[1]Department of Materials Science and Engineering, The Pennsylvania State University, University Park, Pennsylvania

[2]State Key Laboratory of Electrical Insulation and Power Equipment, Xi'an Jiaotong University, Xi'an, Shaanxi, China

[3]State Key Laboratory of Power Transmission Equipment & System Security and New Technology, Chongqing University, Chongqing, China

[4]Faculty of Materials Science and Chemistry, China University of Geosciences, Wuhan, Hubei, China

Correspondence
Qing Wang, Department of Materials Science and Engineering, The Pennsylvania State University, University Park, PA 16802.
Email: wang@matse.psu.edu

Abstract

The exploration of high-energy-density electrostatic capacitors capable of operating both efficiently and reliably at elevated temperatures is of great significance in order to meet advanced power electronic applications. The energy density of a capacitor is strongly dependent on dielectric constant and breakdown strength of a dielectric material. Here, we demonstrate a class of solution-processable polymer nanocomposites exhibiting a concurrent improvement in dielectric constant and breakdown strength, which typically show a negative correlation in conventional dielectric materials, along with a reduction in dielectric loss. The excellent performance is enabled by the elegant combination of nanostructured barium titanate and boron nitride fillers with complementary functionalities. The ternary polymer nanocomposite with the optimized filler compositions delivers a discharged energy density of 2.92 J cm^{-3} and a Weibull breakdown strength of 547 MV m^{-1} at 150°C, which are 83% and 25%, respectively, greater than those of the pristine polymer. The conduction behaviors including interfacial barrier and carrier transport process have been investigated to rationalize the energy storage performance of ternary polymer nanocomposite. This contribution provides a new design paradigm for scalable high-temperature polymer film capacitors.

KEYWORDS

breakdown strength, capacitors, dielectric constant, high temperature, polymer nanocomposites

1 | INTRODUCTION

Dielectric capacitors are ubiquitous components of electric circuits that are utilized to control charges electrostatically via a dielectric material.[1-4] The working principle of electrostatic capacitors involves the repeated electrical polarization and depolarization processes, giving them excellent stability and ultra-fast discharging rates with respect to electrochemical energy storage devices.[5-9] Compared to dielectric ceramics, polymer dielectrics possess intrinsic advantages including lightweight, low cost, and mechanically flexible (critical for coiled capacitor designs), as well as superior electrical breakdown strength and relatively low dielectric loss.[2,10-14]

He Li, Lulu Ren, and Ding Ai contributed equally to this study.

On the other hand, relatively poor thermal stability of polymers limits their high-temperature usages for advanced microelectronics and power systems. For instance, to utilize the state-of-the-art commercial biaxially oriented polypropylene (BOPP) films in power inverters, a separated cooling system has to be installed in electric vehicles in order to reduce operating temperature from ~150°C to ~80°C.[14-16] The additional cooling system not only brings extra weight and volume but also reduces the stability and efficiency of power systems. Recently, engineering polymers with high glass transition temperature (T_g), such as polycarbonate, polyimide (PI), poly(arylene ether nitrile), and poly(ether ketone ketone) have been exploited as high-temperature dielectric materials.[14,17-23] Unfortunately, all the polymers suffer considerable energy loss under high electric fields and at elevated temperatures, which is due to the leakage current that increases exponentially with increasing temperature, resulting in sharp drops in both energy density and charge-discharge efficiency of the polymer dielectrics.

Moreover, compared with electrochemical energy storage devices such as batteries and supercapacitors, the electrostatic capacitors store less energy per unit volume, which fail to meet increasing demands of high energy densities required by advanced energy systems.[9,24] For linear dielectrics, the discharged energy density $U_e = 1/2DE = 1/2\varepsilon_0 KE^2$, where D is the electric displacement, E is the applied electric field, ε_0 is the vacuum permittivity (8.85×10^{-12} F m^{-1}), and K is the dielectric constant. Therefore, U_e is highly dependent on both K and E, where E limited by the breakdown strength of dielectrics.[25,26] To enhance U_e, extensive studies have been carried out to improve K by adding high K ceramic fillers such as barium titanate (BT), barium strontium titanate, and copper titanate calcium into polymer matrices.[27-32] However, the thus-designed polymer composites typically suffer from large reductions in breakdown strength, which preclude a substantial gain in U_e. Alternatively, wide-band-gap fillers such as aluminum oxide (Al_2O_3), silicon dioxide (SiO_2), and boron nitride (BN) have been utilized to enhance breakdown strength of polymer composites.[33-37] For instance, a library of BN nanosheets (BNNSs)-based polymer nanocomposites have been prepared by using various polymer matrices including poly(vinylidene fluoride-triuoroethylene-chlorouoroethylene), poly(methyl methacrylate), poly(ether imide) (PEI), and crosslinked divinyltetramethyldisiloxane-bis(benzocyclobutene) (*c*-BCB).[14,38-41] Synergistic enhancements in breakdown strength, mechanical strength, and thermal conductivity along with reduced electric conductivity and lowered loss tangent (tan δ) are achieved in the resultant nanocomposites. It is well recognized that K and breakdown strength show a negative correlation in conventional dielectric materials. Numerous efforts such as construction of the core-shell structured fillers[42-44] and design of multilayered films[45-49] have been performed to enhance both K and breakdown strength of dielectric composites. However, the complex fabrication processes limit scalability of these approaches.

Herein, we report a solution-processable PEI nanocomposites consisting of two inorganic fillers with complementary functionalities, including BNNSs with high dielectric strength and BT nanoparticles (BTNPs) with large electric polarization. Concurrent enhancements in both K and breakdown strength have been achieved in the resulting ternary polymer nanocomposites, which lead to outstanding electrical storage and discharging performance in comparison with pristine PEI and other engineering polymer films and excellent cyclability at elevated temperatures.

2 | METHODS

2.1 | Materials fabrication

BNNSs were fabricated via a modified liquid-phase exfoliation method.[50] 4 g *h*-BN powders (Sigma Aldrich) were dispersed in 300 mL *N*,*N*-dimethylformamide (Sigma Aldrich) and exfoliated using a tip-type ultrasonic disruptor (175 W, 500 W × 35%) for 48 hours. The resulting mixture was first centrifuged at 3000 rpm for 40 minutes to purify the mixture from un-exfoliated *h*-BN powders. Then the purified supernatant was centrifuged at 10 000 rpm for 20 minutes to collect BNNSs from solvent. The products were dried at 70°C overnight in a vacuum oven.

Binary PEI/BTNP and PEI/BNNS and ternary PEI/BTNP/BNNS nanocomposite films were fabricated through solution casting processes. PEI pellets were incorporated into *N*-methylpyrrolidone (NMP; Sigma Aldrich) and vigorously magnetic stirred overnight to yield a clear and transparent solution. The nanofillers of BTNP (average particle diameter of 100 nm, US Research Nanomaterials, Inc.) and BNNS dispersion with varied concentrations were prepared in NMP by tip-type ultrasonication (175 W, 500 W × 35%) for 1 hour, respectively. The binary PEI/BTNP and PEI/BNNS mixtures were obtained by mixing PEI solution with nanofiller dispersion. Similarly, the ternary PEI/BTNP/BNNS mixtures were yielded through introducing both BTNP and BNNS dispersions into PEI solution. All the mixtures were further sonicated for another 30 minutes before casting onto a clean glass substrate. The schematic fabrication process of the films is shown in Figure 1. Afterwards, the solution-casted nanocomposite films were dried at 120°C for 12 hours, and subsequently peeled off from the substrates in deionized water followed by drying at 120°C for another 12 hours in a vacuum oven

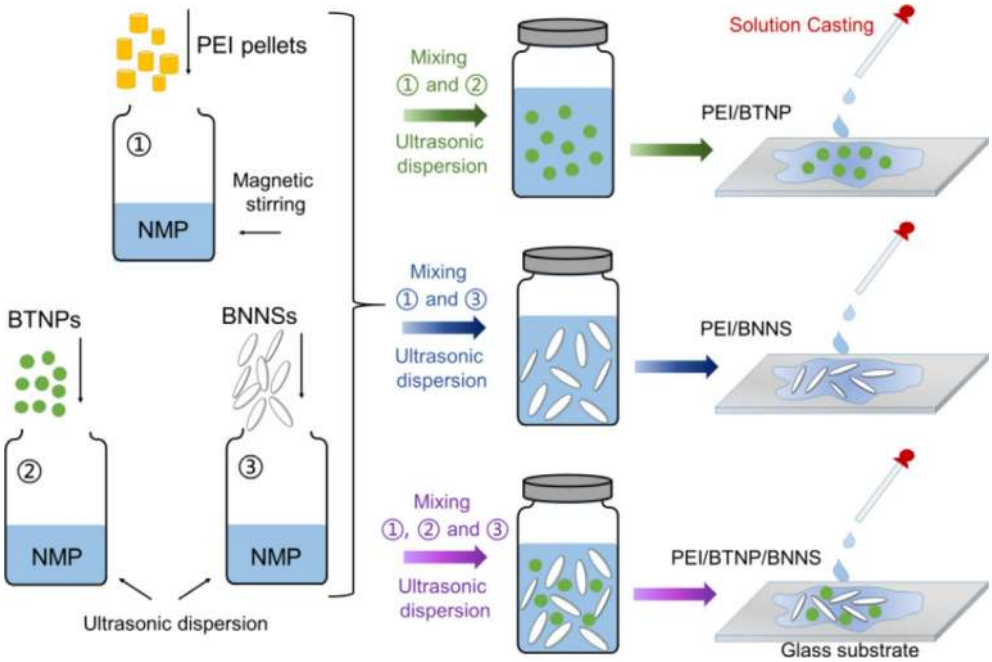

FIGURE 1 Schematic of the preparation of the poly(ether imide) (PEI)-based nanocomposite films

to remove solvent residue and water. The typical thickness of nanocomposite films is 8-14 μm.

2.2 | Characterization

Transmission electron microscopy (TEM) images were collected using a FEI Talos F200X transmission electron microscopy by firstly placing a few drops of dispersion on a lacey carbon covered copper grid and then evaporating it prior to observation. Scanning electron microscopy (SEM) images of cross-sectional morphologies were obtained using a FEI NanoSEM 630 Field emission scanning electron microscope. The element mapping images were obtained using an energy-dispersive spectroscopy (EDS) attached to SEM. Fourier transform infrared (FTIR) spectra were recorded by a Varian Digilab FTS-8010 spectrometer at room temperature. Polymeric films were collected in the attenuated total reflectance mode using ZnSe crystal as a contact to the samples, and nanofillers were mixed with potassium bromide (KBr) and collected in the transmission mode. X-ray diffraction (XRD) analysis was carried out by a PANalytical X'pert Pro MPD theta-theta diffractometer. Dielectric spectra were recorded using a Hewlett Packard 4284A LCR meter within a broad frequency range of 10^2 to 10^6 Hz and at varied temperatures. Direct-current (DC) steady state conduction currents were obtained under an electric field of 100 MV m^{-1} using a Hewlett Packard 4140B pA meter/DC voltage source with External Trek 1010BHS amplifier as a high-voltage source in conjunction with a Delta Design 9023 oven equipped with a liquid nitrogen cooling system. DC volume conductivities were calculated based on the conduction current results. Dielectric breakdown strength measurements were carried out using a TREK P0621P instrument according to an electrostatic pull-down method under a DC voltage ramp of 500 V s^{-1}. The breakdown field from 15 measurements was determined based on a two-parameter Weibull statistic described as:

$$P(E) = 1 - \exp\left(-(E/E_b)^{\beta}\right) \tag{1}$$

where $P(E)$ is the cumulative probability of electric failure, E is the measured breakdown field, E_b (Weibull breakdown strength) is the characteristic breakdown strength that corresponds to a 63.2% probability of failure, and the shape parameter β evaluates the scatter of data. High field displacement-electric field (*D-E*) loops were collected using a modified Sawyer-Tower circuit with a high-voltage amplifier system, using a triangular unipolar wave with a frequency of 10 Hz. The charged energy density (U_c) is derived from the *D-E* loop by integration of the area between the charge curve and the ordinate, and the discharged energy density (U_e) is determined by the area between the discharge curve and ordinate, accordingly, the charge-discharge efficiency (η) can be calculated from $\eta = U_e/U_c$. Fast discharge tests were carried out using a PK-CPR1502 test system equipped with a Behlke HTS81 high-voltage metal oxide semiconductor field-effect transistor switch. The resistance of the load resistor is 6.5 kΩ and the charge-discharge cycles were controlled by a LabVIEW program. All the breakdown, *D-E* loop, and fast discharge

measurements were performed in Galden HT insulation fluid. The temperature was controlled by a digital hot plate equipped with a thermal couple. For all the electrical measurements, gold electrodes with a thickness of around 60 nm were sputtered on both sides of the polymeric films.

3 | RESULTS AND DISCUSSION

3.1 | Structural characterizations

As shown in the TEM image of the exfoliated BNNS (Figure 2A), the thickness of BNNS is around 2.2 nm with 2 to 6 layers. The width of the nanosheets is around 400 to 600 nm as demonstrated in our previous works.[14,25,26,40] The XRD curves of *h*-BN and BNNS are presented in Figure S1, the shape characteristic peak at $2\theta = 26.7°$ refers to the hexagonal symmetry of (002) BN, which evidences that the exfoliation process does not change the crystal structures of *h*-BN. Figure 2B,C show the cross-sectional images of the PEI nanocomposite films filled with BTNPs and BNNSs, respectively, indicating that the inorganic fillers are well dispersed in PEI matrix. Stable ternary suspensions in NMP at a relatively high concentration of 25:1.5:2.5 mg mL^{-1} of PEI to BTNPs to BNNSs is shown in Figure 2D. It can be seen from Figure 2E that the nanocomposite film displays excellent mechanical flexibility even at a relatively high filler concentration, for example, 1.27 vol% BTNPs and 6.05 vol% BNNSs. The cross-sectional morphology of the ternary nanocomposite is exhibited in Figure 2F, in which the homogeneous filler dispersion is verified by the EDS mapping of different element distributions (Figure 2G). Different from conventional polymer composites that usually require surface functionalization of inorganic fillers to achieve uniform filler dispersion in polymer matrix,[8,51,52] the direct use of pristine fillers without any surface modification would not only simplify the preparation of the polymer nanocomposites but also greatly benefit the breakdown strength of the composites. For the polymer composites filled with surface-functionalized fillers, the modification agents are typically long hydrocarbon chains, which is the region most vulnerable to the applied high electric field due to their lowest *K* in comparison with polymer matrices and inorganic phases.[25,38] In addition, the thermal-dielectric stability of the grafted ligands and molecular chain segments is inferior to that of high-temperature PEI matrix and inorganic fillers, which would contribute to dielectric loss especially at elevated temperatures, for example, >150°C and under high electric fields. Figures S2 and

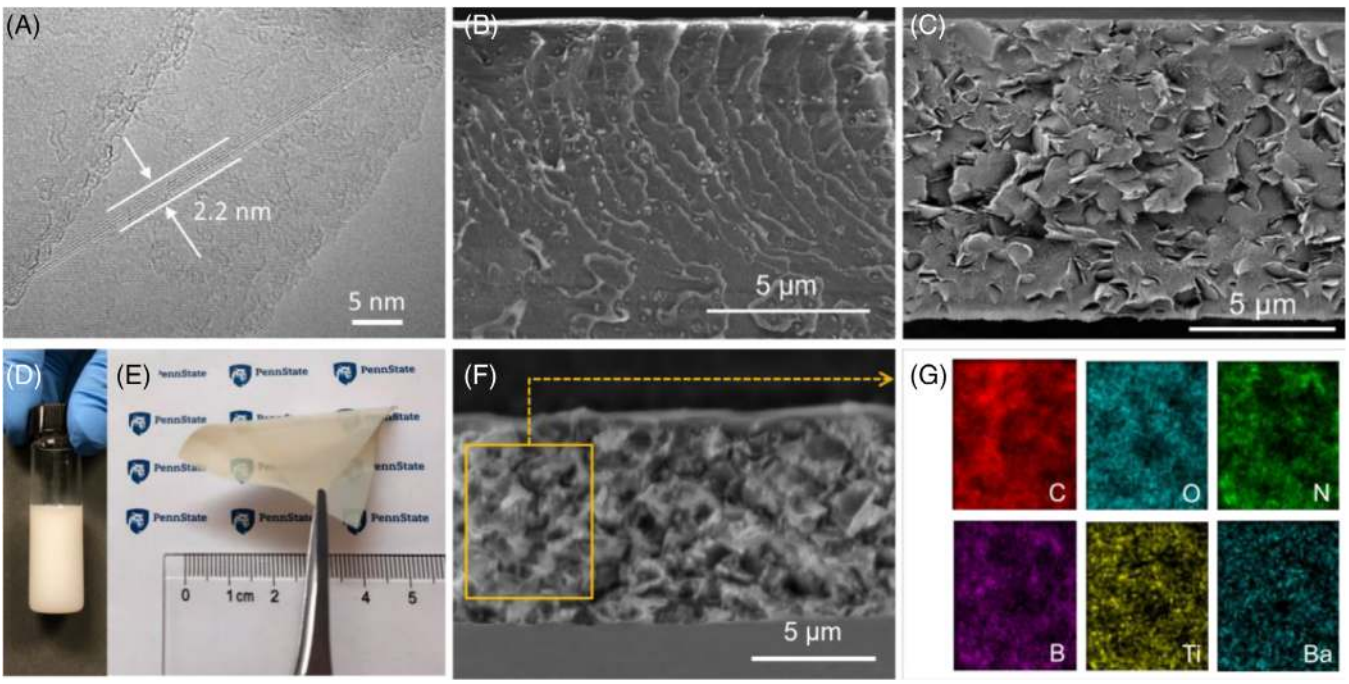

FIGURE 2 A, TEM image of BNNS with exposed edge showing the layer structure. B, Cross-sectional SEM image of the PEI nanocomposite with 1.27 vol% BTNPs. C, Cross-sectional SEM image of the PEI nanocomposite with 6.05 vol% BNNSs. D, Photograph of PEI pellet, BTNP and BNNS dissolved in NMP. E, Photograph of a bent ternary PEI nanocomposite film containing 1.27 vol% BTNPs and 6.05 vol% BNNSs. F, Cross-sectional SEM image of the ternary PEI nanocomposite with 1.27 vol% BTNPs and 6.05 vol% BNNSs. G, Element mapping of carbon (C), oxygen (O), nitrogen (N), boron (B), titanium (Ti) and barium (Ba) on the orange-marked area in F established using EDS. BNNSs, BN nanosheets; BTNPs, BT nanoparticles; NMP, *N*-methylpyrrolidone; PEI, poly(ether imide); SEM, scanning electron microscopy; TEM, Transmission electron microscopy

S3 show the FTIR and XRD curves of BNNS, BTNP, PEI, and ternary PEI nanocomposite consisting 1.27 vol% BTNPs and 6.05 vol% BNNSs, respectively, indicating that the addition of multiple inorganic fillers does not change the chemical structure and the amorphous nature of PEI.

3.2 | Dielectric properties of binary nanocomposites

The frequency-dependent dielectric spectra of binary PEI/BTNP and PEI/BNNS nanocomposites are shown in Figure S4. Figure 3A,B summarize the K and tan δ as a function of BTNP and BNNS filler content, respectively. The K of both binary nanocomposites increases with increasing filler content, for example, from 3.26 of the neat PEI to 3.82 of PEI/BTNP with 1.69 vol% fillers, to 3.44 of PEI/BNNS with 8.47 vol% fillers at 10^3 Hz and room temperature. As excepted, BTNP fillers give rise to higher K of the composites relative to the PEI filled with the same content of BNNS, which is attributed to the greater K of BT comparing with BN (>60 vs 4-4.5).[7,9,10] As the inorganic fillers with higher K usually exhibit greater dielectric loss, tan δ of the composites increases from 0.0084 of the neat PEI to 0.0117 of the PEI composite with 1.69 vol% BNTP fillers. Conversely, the addition of wide band-gap (~6 eV) BNNS fillers can effectively reduce tan δ of the composites,[14,38,39] which reaches the minimum value of 0.0053 at 7.26 vol% filler content.

It is known that the breakdown behavior of nanocomposites is largely dependent on the morphology of incorporated fillers.[33,53] In general, the parallel two-dimensional nanosheets are effective in dispersing the applied electric field throughout the polymer matrix to mitigate the inhomogeneous distribution of local electric fields. For the composite filled with zero-dimensional nanoparticles, the electric fields are highly concentrated around the fillers, leading to the easy formation of discharging channels and consequently compromised E_b. Figure S5 presents the Weibull statistics of dielectric breakdown strength of the PEI/BTNPs and PEI/BNNSs nanocomposites measured at room temperature. The E_b and β are summarized in Figure 4A,B, respectively, as a function of BTNP and BNNS filler contents. The monotonic decrease in E_b and β value of the BTNP-containing composites with increasing filler loading is associated with the lower dielectric strength and larger dielectric loss of BT as well as large contrast in K between organic and inorganic phases. On the contrary, the E_b of PEI/BNNSs nanocomposites achieves the peak value of 638 MV m^{-1} at 6.05 vol% filler feeding ratio, which represents almost 30% enhancement as compared to that of neat PEI. Meanwhile, a pronounced increase of β value is found from 10.79 of neat PEI to 15.17 of the PEI nanocomposite with 7.26 vol% BNNSs, indicative of higher dielectric reliability of the nanocomposite. The further addition of the BNNS fillers into PEI leads to concomitant reductions in E_b and β, which is mainly attributed to filler aggregations and interfacial defects as evidenced by cross-sectional SEM image of 8.47 vol% BNNS-filled PEI composite film (Figure S6).

Figure S7 presents the η of binary PEI/BTNP and PEI/BNNS nanocomposites with varied filler loadings, which show a strong dependence on the filler content. For instance, the incorporation of BTNP fillers sequentially decreases η whereas the PEI/BNNS nanocomposite with 6.05 vol% filler loading achieves the highest η among all the feeding ratios. It is seen that the relatively high loss of the BT-containing composites leads to a sharply reduction in η. On the other hand, the relatively low K of BNNS precludes a substantial gain in electric displacement of the polymer composites. Therefore, the use of these two fillers

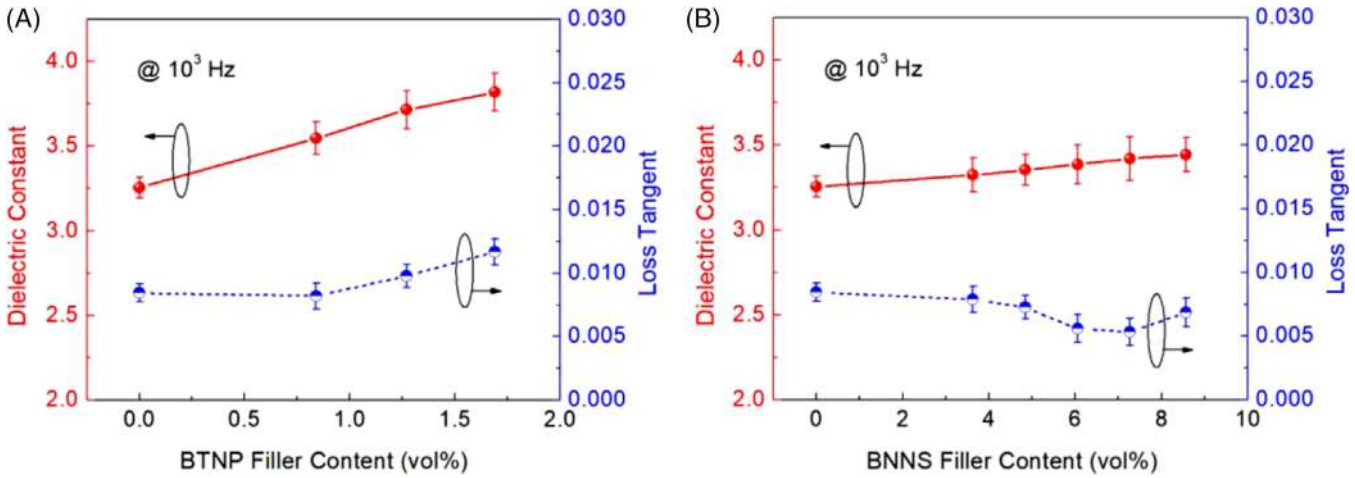

FIGURE 3 Dielectric constant and loss tangent of the binary PEI nanocomposites as a function of A, BTNP filler content and B, BNNS filler content measured at room temperature and 10^3 Hz. BNNS, BN nanosheets; BTNP, BT nanoparticle; PEI, poly(ether imide)

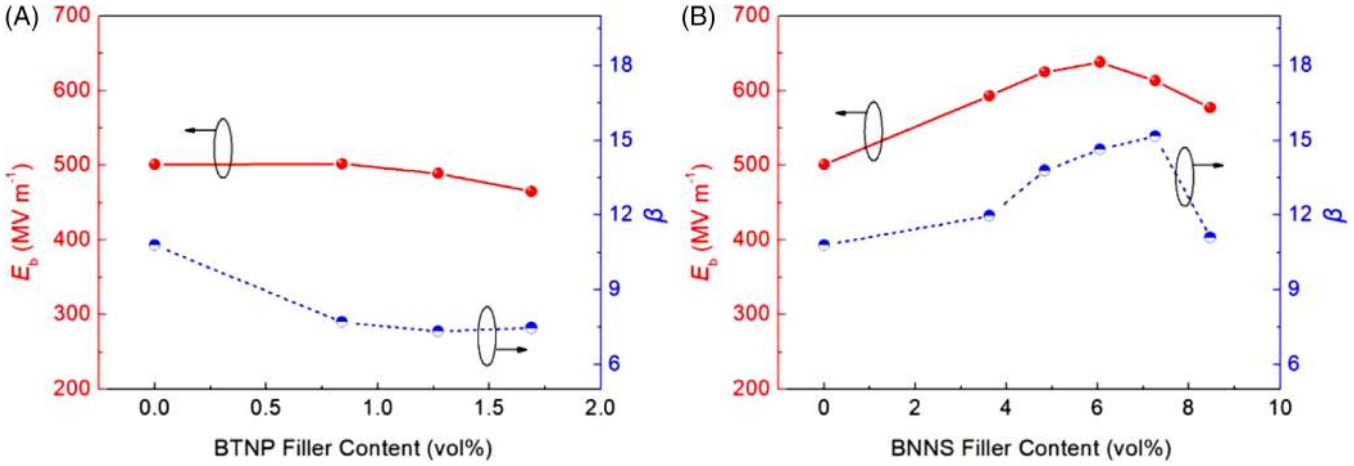

FIGURE 4 E_b and β value of the binary PEI nanocomposites as a function of A, BTNP filler content and B, BNNS filler content measured at room temperature. BNNS, BN nanosheet; BTNP, BT nanoparticle; PEI, poly(ether imide)

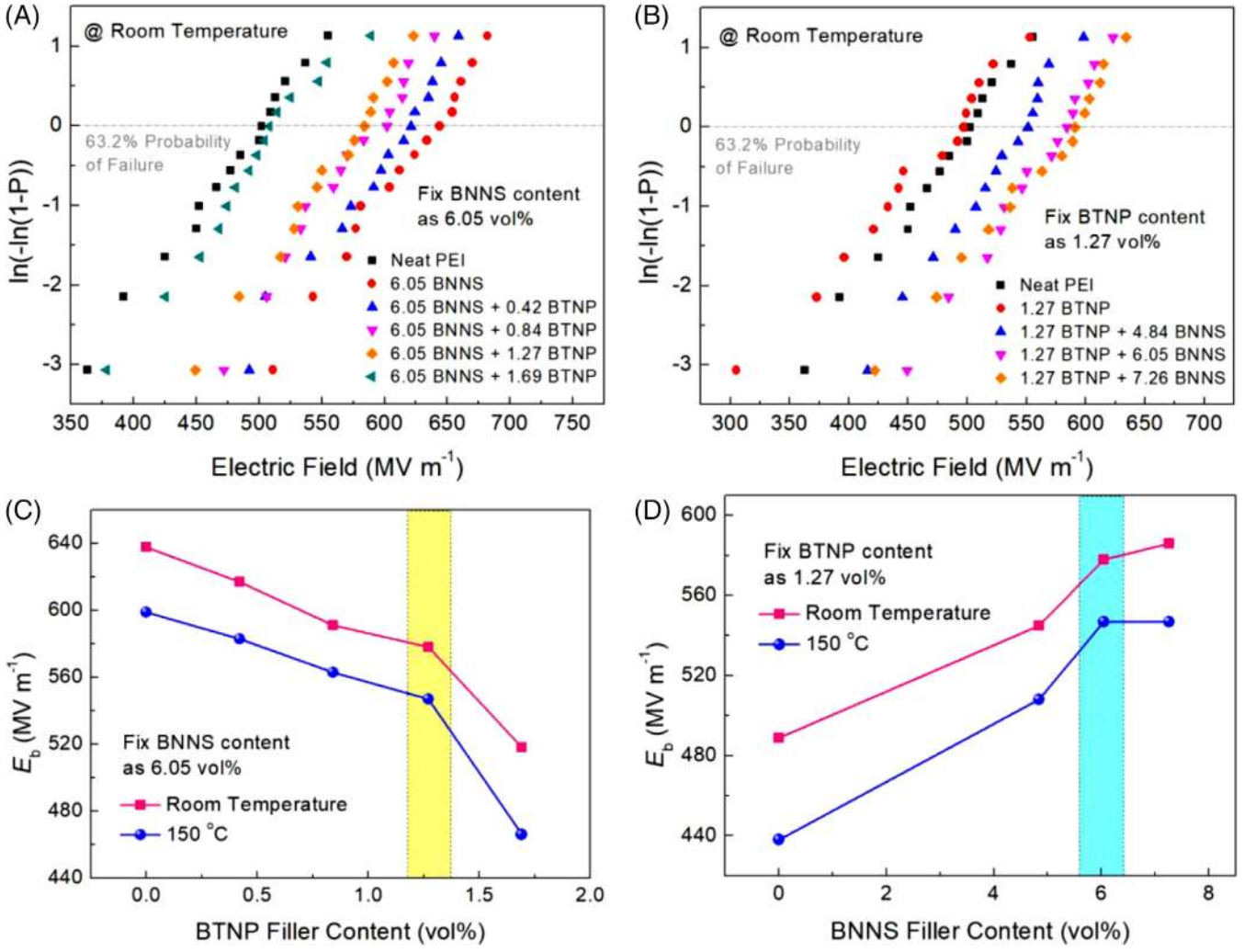

FIGURE 5 Weibull plots of dielectric breakdown strength of the ternary PEI nanocomposites with A, 6.05 vol% BNNS filler content and B, 1.27 vol% BTNP filler content at room temperature. E_b of the ternary PEI nanocomposites with C, 6.05 vol% BNNS loading as a function of BTNP filler content and D, 1.27 vol% BTNP loading as a function of BNNS filler content. BNNS, BN nanosheet; BTNP, BT nanoparticle; PEI, poly(ether imide)

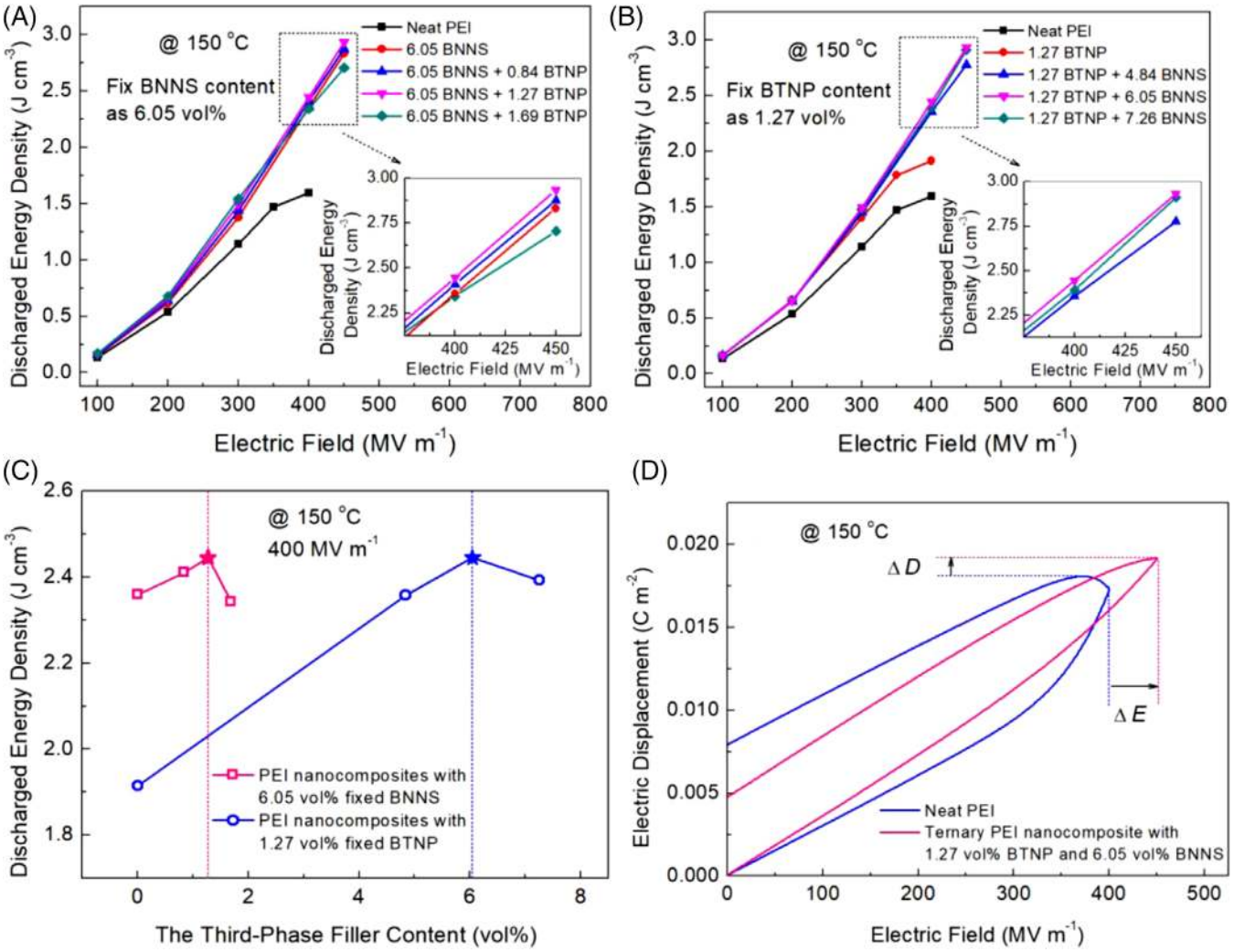

FIGURE 6 Discharged energy density of the ternary PEI nanocomposites with A, 6.05 vol% BNNS filler content and B, 1.27 vol% BTNP filler content as a function of electric fields at 150°C. Insets show the partial enlarged details of the dotted box in (A) and (B). C, discharged energy density of the ternary PEI nanocomposites with 6.05 vol% BNNS loading and 1.27 vol% BTNP loading, respectively, as a function of the third-phase filler content at 150°C and under 400 MV m^{-1}. D, *D-E* loops of neat PEI and the ternary PEI nanocomposite containing 1.27 vol% BTNP and 6.05 vol% BNNS at 150°C. BNNS, BN nanosheet; BTNP, BT nanoparticle; PEI, poly(ether imide)

individually limits the further increment of the energy density of electrostatic capacitors. To achieve concurrent enhancements in both η and electric displacement, BTNPs along with BNNSs were synergistically included in PEI to create ternary PEI/BTNP/BNNS nanocomposites.

3.3 | Dielectric properties of ternary nanocomposites

A library of the ternary PEI/BTNP/BNNS nanocomposites consisting of multiple nanostructured inorganic fillers with varied feeding ratios has been prepared. We first conducted systematic investigation on the dielectric breakdown strength of the ternary PEI composites with 6.05 vol% BNNSs and varied BTNP feeding ratios, since the highest E_b was achieved in the binary PEI/BNNS system with an optimal content of 6.05 vol% BNNSs. Weibull statistics of dielectric breakdown strength of the ternary PEI nanocomposites with 6.05 vol% BNNSs measured at room temperature and 150°C are shown in Figures 5A and S8A, respectively, and E_b values are summarized in Figure 5C as a function of filler content. As can be seen in Figure 5C, the incorporation of BTNPs leads to the initial decrease in E_b. With further increase of BTNP filler content beyond 1.27 vol%, E_b exhibits a steeply fall which seems to be a threshold that the BTNP fillers gradually start to connect with each other and thus result in vulnerable regions against breakdown process. To find out the optimum ratio of the inorganic fillers, we fix the threshold-liked ratio of 1.27 vol%, for BTNPs and vary the BNNS content in the ternary nanocomposites. As shown in Figure 5B and Figure S8B, the E_b of the ternary composites increase with increasing BNNS filler content but β value

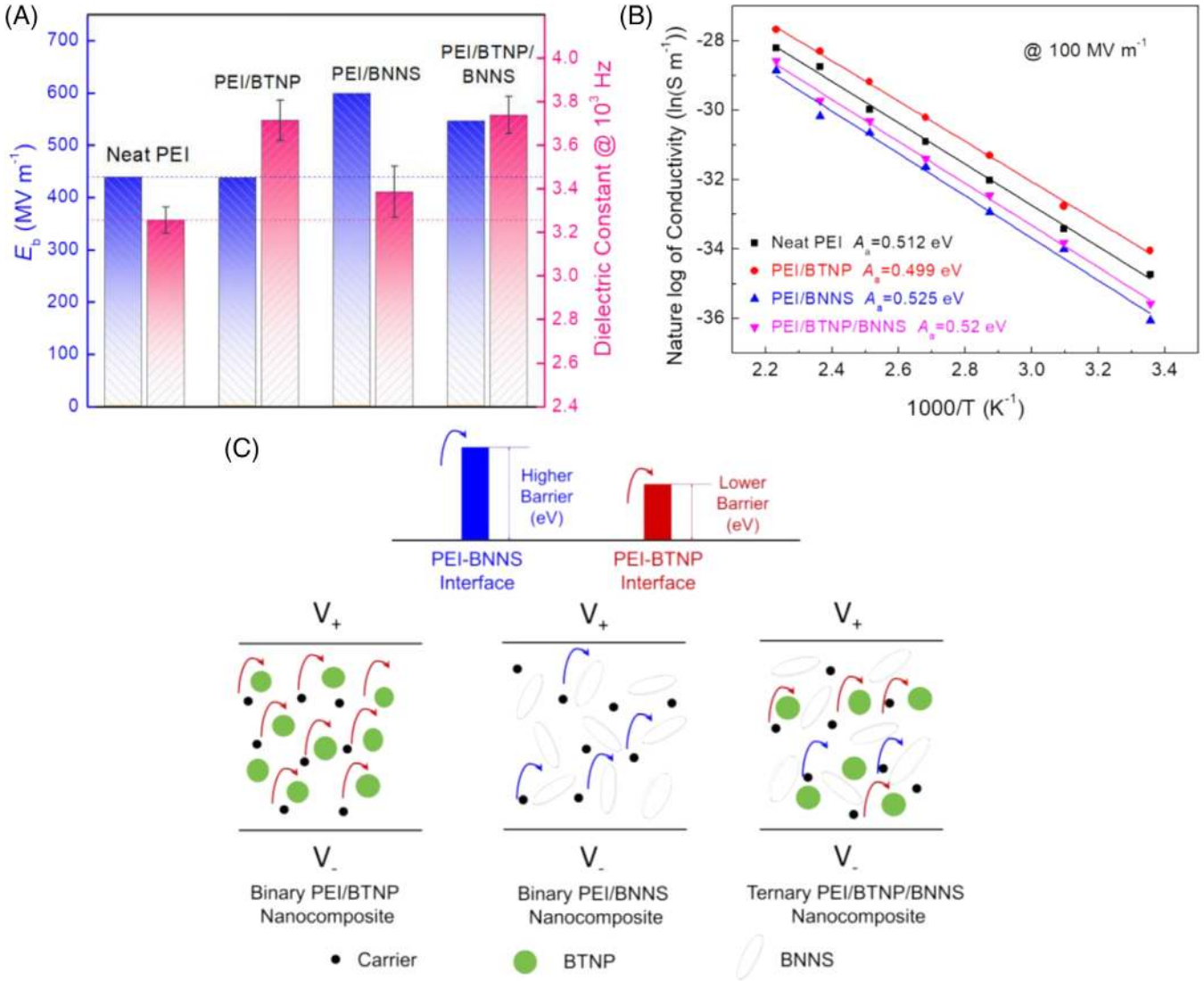

FIGURE 7 A, Comparison of the Weibull breakdown strength at 150°C and the dielectric constant at 10^3 Hz and room temperature of neat PEI, the binary PEI/BTNP nanocomposite with 1.27 vol% BTNP, the binary PEI/BNNS nanocomposite with 6.05 vol% BNNS and the ternary PEI nanocomposite with 1.27 vol% BTNPs and 6.05 vol% BNNSs. B, Arrhenius plots of electrical conductivity of neat PEI, the binary PEI/BTNP nanocomposite with 1.27 vol% BTNPs, the binary PEI/BNNS nanocomposite with 6.05 vol% BNNSs and the ternary PEI nanocomposite with 1.27 vol% BTNPs and 6.05 vol% BNNSs under 100 MV m^{-1}. C, Schematics of the interfacial barrier and the carrier transport process of the PEI-based nanocomposites. BNNS, BN nanosheet; BTNPs, BT nanoparticles; PEI, poly(ether imide)

starts to fall when the feeding ratio of BNNS is more than 6.05 vol% (Table S1). The reduction in β is likely due to the agglomeration of inorganic fillers at high loadings. The inflection points highlighted in Figure 5D further evidence a balanced content of these two complementary fillers, that is, 1.27 vol% BTNPs and 6.05 vol% BNNSs, in the ternary system. As seen in the frequency-dependent dielectric spectra of the ternary composites (Figure S9), both K and tan δ increase with increasing BTNP filler content of the ternary PEI nanocomposites with 6.05 vol% BNNSs. By sharp contrast, the addition of the BNNS fillers in the ternary nanocomposites not only effectively suppresses dielectric loss but also simultaneously retains the high K value that induced by BTNP fillers. These results indicate that the key dielectric characteristics of K and E_b could be readily tailored by varying the composite compositions. Figure S10 presents the temperature dependence of dielectric spectra of neat PEI and the composites. The binary and ternary nanocomposites retain the distinct weak-field dielectric properties of PEI, for example, stable K over a temperature range of 25°C to 200°C, indicative of minimized impacts of BTNP and BNNS fillers on the temperature-dependent properties of the PEI-based composites.

Capacitive performances of the ternary PEI nanocomposites with multiple nanostructured inorganic fillers of BTNP and BNNS have been systematically investigated. As

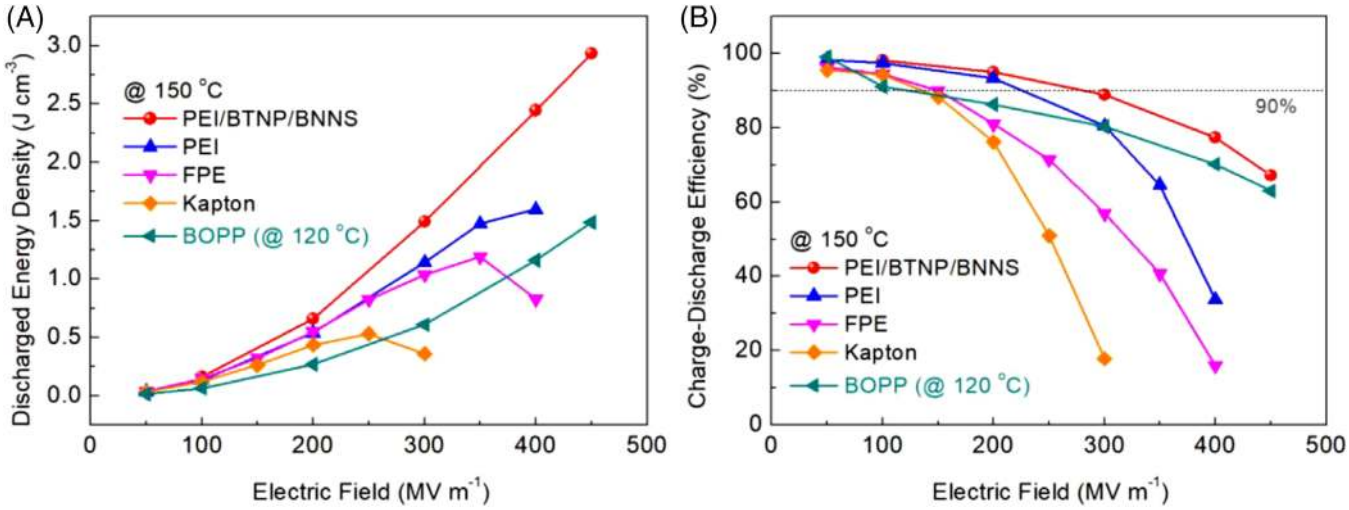

FIGURE 8 A, Discharged energy density and B, charge-discharge efficiency of commercial dielectric polymers and the ternary PEI nanocomposite with 1.27 vol% BTNPs and 6.05 vol% BNNSs. BNNSs, BN nanosheets; BOPP, biaxially oriented polypropylene; BTNPs, BT nanoparticles; FPE, fluorine polyester; PEI, poly(ether imide)

shown in Figure 6A,B, the ternary system filled with 1.27 vol% BTNPs and 6.05 vol% BNNSs gives rise to the highest U_e among all the binary and ternary systems. Figure 6C compares the U_e of the PEI nanocomposites with varied third-phase filler content measured at 150°C and 400 MV m^{-1}. As excepted, the highest U_e of 2.45 J cm^{-3} is achieved from the composition of 1.27 vol% BTNPs and 6.05 vol% BNNSs, which further verified the optimized filler compositions of ternary PEI/BTNP/BNNS nanocomposites. From the comparison in *D-E* hysteresis loops of neat PEI and the ternary PEI nanocomposite with 1.27 vol% BTNPs and 6.05 vol% BNNSs (Figures 6D and S11), it is evident that the incorporated fillers drastically narrow the loops while retaining the electric displacement. Notably, as seen in Figure 6D, concomitant enhancements in both electric displacement and the strength of the applied electric field are presented in the loops of the ternary nanocomposite with respect to that of neat PEI, owing to the synergetic effects from the introduced BTNP and BNNS fillers with complementary functionalities. Moreover, the existence of BNNSs suppresses the leakage current under high electric fields, leading to lower remnant polarization and higher η of the ternary composites.

Figure 7A compares K and E_b of neat PEI, binary 1.27 vol% BTNP-filled PEI, 6.05 vol% BNNS-filled PEI nanocomposite, and the ternary PEI nanocomposite with 1.27 vol% BTNPs and 6.05 vol% BNNSs. A high K of 3.74 along with a low tan δ of 0.00715 at 10^3 Hz and room temperature as well as an outstanding E_b of 547 MV m^{-1} measured at 150°C are obtained in the ternary PEI nanocomposite, significantly outperforming pristine PEI. It is known that electrical conduction plays a critical role in dielectrics operating at elevated temperatures and high electric fields. Therefore, we investigated the conduction behaviors of the composites at a relatively high electric field, for example, 100 MV m^{-1}, at varied temperatures as shown in Figure 7B. The activation energy is determined from the temperature dependence of electrical conductivity, which typically fits an Arrhenius relationship given as:

$$\sigma(T) = \sigma_0 * \exp\left(-\frac{A_a e}{K_B T}\right) \tag{2}$$

where σ_0 is the prefactor, A_a is the activation energy in eV, e is the electronic charge of carriers, and K_B is the Boltzmann constant. Compared with neat PEI, the activation energy of BTNP-filled binary composite decreases from 0.512 eV to 0.499 eV. In contrast, the addition of BNNSs increases the activation energy to 0.525 eV, which is attributed to a higher barrier at the interface between polymer matrix and BNNS than that of BTNP (Figure 7C). In the rationally designed ternary composites, BNNSs not only give rise to a higher energy barrier for the carrier to overcome during conduction process because of their wide bandgap but also effectively block the connection of BTNPs, thus ensuring the ternary polymer composites to maintain excellent dielectric strength.

The ternary PEI/BTNP/BNNS nanocomposite with the optimized filler concentration possesses the best U_e among the PEI-based binary and ternary nanocomposites as compared above, and also exhibits great high-temperature capabilities in both U_e and η with respect to other commercial high-temperature polymer films including fluorine polyester (FPE), Kapton PI, and the state-of-the-art polymer dielectric

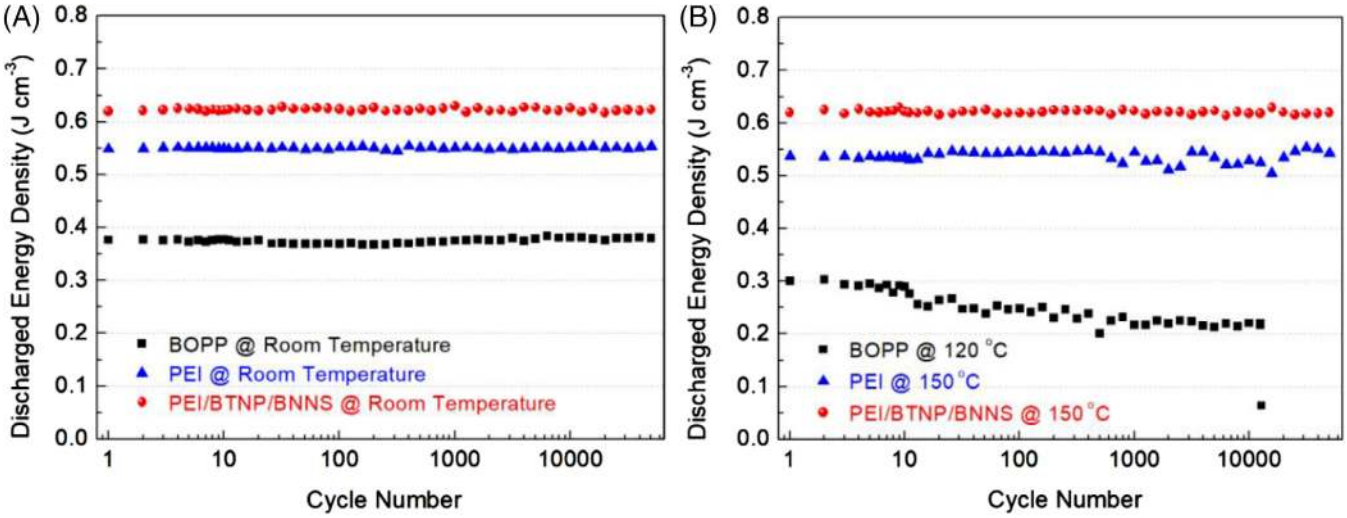

FIGURE 9 Discharged energy density of BOPP, PEI, and the ternary PEI nanocomposite with 1.27 vol% BTNPs and 6.05 vol% BNNSs at A, room temperature and B, elevated temperatures measured under 200 MV m^{-1} as a function of cycle numbers. BNNSs, BN nanosheets; BOPP, biaxially oriented polypropylene; BTNPs, BT nanoparticles; PEI, poly(ether imide)

film—BOPP,[16,34] as shown in Figure 8. Note that the results for BOPP is collected at 120°C due to its relatively low melting temperature of ~165°C.[40] At 150°C, the ternary PEI nanocomposite with 1.27 vol% BTNPs and 6.05 vol% BNNSs delivers the highest U_e of 2.92 J cm^{-3} vs 1.6 J cm^{-3} of neat PEI and 1.19 J cm^{-1} of FPE. Remarkably, the ternary nanocomposite maintains a η of almost 90% under a high field of 300 MV m^{-1}.

To evaluate the stability of the ternary nanocomposite films over continuous charge-discharge processes, the cyclic fast discharge tests have been conducted at ambient and elevated temperature at an applied filed of 200 MV m^{-1} as shown in Figure 9. Impressively, the ternary nanocomposite with 1.27 vol% BTNPs and 6.05 vol% BNNSs presents almost no sign of degradation in U_e over a straight 50 000 cycles at both room temperature and 150°C. In contrast, while neat PEI and BOPP remain stable at room temperature throughout the whole cycle range, noticeable variations of U_e appears when the temperature increases. As shown in Figure 9B, the PEI film displays a variation of U_e of over 9% within 50 000 cycles at 150°C, and the BOPP film is broken down at the 12 852nd cycle at 120°C.

4 | CONCLUSION

In summary, we demonstrate substantially enhanced energy density and charge-discharge efficiency in rationally designed ternary polymer nanocomposite films with multiple ceramic nanofillers. Owing to the coexistence of BTNP fillers with large electric displacement and BNNS fillers with ultra-high insulting strength, two key dielectric characteristics of K and E_b have been readily tailored by simply varying the composite compositions. Along with the decreased high-field dielectric loss, the ternary PEI/BTNP/BNNS nanocomposites with optimized filler feeding ratios yield vastly enhanced high-temperature capacitive performance. The excellent charge-discharge efficiency and outstanding cyclability achieved under high electric fields and at elevated temperatures demonstrate the feasibility of the ternary polymer nanocomposite films for applications in high-temperature electrostatic capacitors. Compared with the current designs of multiphased polymer nanocomposites, for example, core@shell-structured fillers and sandwich-structured films. The approach we describe herein possesses the advantage of facile preparation and thus offers a general design paradigm of the combination of complementary nanostructured fillers for polymer nanocomposites to boost their comprehensive properties.

ACKNOWLEDGMENTS

H. Li, L. Ren, and D. Ai acknowledge the support from the China Scholarship Council (CSC).

CONFLICT OF INTEREST

The authors have no conflict of interest to report.

ORCID

He Li https://orcid.org/0000-0002-4076-7279
Qing Wang https://orcid.org/0000-0002-5968-3235

REFERENCES

1. Karden E, Ploumen S, Fricke B, Miller T, Snyder K. Energy storage devices for future hybrid electric vehicles. *J Power Sources*. 2007;168:2-11.
2. Wang Y, Zhou X, Chen Q, Chu B, Zhang QM. Recent development of high energy density polymers for dielectric capacitors. *IEEE Trans Dielectr Electr Insul*. 2010;17:1036-1042.
3. Tan Q, Irwin P, Cao Y. Advanced dielectrics for capacitors. *IEEJ Trans Fund Mater*. 2006;126:1152-1159.
4. Ho J, Jow TR, Boggs S. Historical introduction to capacitor technology. *IEEE Electr Insul Mag*. 2010;26:20-25.
5. Chu B, Zhou X, Ren K, et al. A dielectric polymer with high electric energy density and fast discharge speed. *Science*. 2006;313:334-336.
6. Wang Q, Zhu L. Polymer nanocomposites for electrical energy storage. *J Polym Sci Poly Phys*. 2011;49:1421-1429.
7. Dang ZM, Yuan J, Yao S, Liao R. Flexible nanodielectric materials with high permittivity for power energy storage. *Adv Mater*. 2013;25:6334-6365.
8. Li Q, Yao FZ, Liu Y, Zhang G, Wang H, Wang Q. High-temperature dielectric materials for electrical energy storage. *Ann Rev Mater Res*. 2018;48:219-243.
9. Li H, Liu F, Fan B, Ai D, Peng Z, Wang Q. Nanostructured ferroelectric-polymer composites for capacitive energy storage. *Small Methods*. 2018;2:1700399.
10. Yao Z, Song Z, Hao H, et al. Homogeneous/inhomogeneous-structured dielectrics and their energy-storage performances. *Adv Mater*. 2017;29:1601727.
11. Pan H, Ma J, Ma J, et al. Giant energy density and high efficiency achieved in bismuth ferrite-based film capacitors via domain engineering. *Nat Commun*. 2018;9:1813.
12. Khanchaitit P, Han K, Gadinski MR, Li Q, Wang Q. Ferroelectric polymer networks with high energy density and improved discharged efficiency for dielectric energy storage. *Nat Commun*. 2013;4:2845.
13. Zhu L, Wang Q. Novel ferroelectric polymers for high energy density and low loss dielectrics. *Macromolecules*. 2012;45:2937-2954.
14. Li Q, Chen L, Gadinski MR, et al. Flexible high-temperature dielectric materials from polymer nanocomposites. *Nature*. 2015;523:576-579.
15. Rabuffi M, Picci G. Status quo and future prospects for metallized polypropylene energy storage capacitors. *IEEE Trans Plasma Sci*. 2002;30:1939-1942.
16. Zhou Y, Li Q, Dang B, et al. A scalable, high-throughput, and environmentally benign approach to polymer dielectrics exhibiting significantly improved capacitive performance at high temperatures. *Adv Mater*. 2018;30:1805672.
17. Johnson RW, Evans JL, Jacobsen P, Thompson JR, Christopher M. The changing automotive environment: high-temperature electronics. *IEEE Trans Electron Packag Manuf*. 2004;27:164-176.
18. Zhang Z, Wang DH, Litt MH, Tan L-S, Zhu L. High-temperature and high-energy-density dipolar glass polymers based on sulfonylated poly(2,6-dimethyl-1,4-phenylene oxide). *Angew Chem Int Ed*. 2018;130:1544-1547.
19. Pan J, Li K, Li J, Hsu T, Wang Q. Dielectric characteristics of poly(ether ketone ketone) for high temperature capacitive energy storage. *Appl Phys Lett*. 2009;95:022902.
20. Wang DH, Kurish BA, Treufeld I, Zhu L, Tan L-S. Synthesis and characterization of high nitrile content polyimides as dielectric films for electrical energy storage. *J Polym Sci Poly Chem*. 2015;53:422-436.
21. Fan B, Liu F, Yang G, et al. Dielectric materials for high-temperature capacitors. *IET Nanodielectr*. 2018;1:32-40.
22. Ho JS, Greenbaum SG. Polymer capacitor dielectrics for high temperature applications. *ACS Appl Mater Interfaces*. 2018;10:29189-29218.
23. Burlingame Q, Wu S, Lin M, Zhang QM. Conduction mechanisms and structure-property relationships in high energy density aromatic polythiourea dielectric films. *Adv Energy Mater*. 2013;3:1051-1055.
24. Thakur VK, Gupta RK. Recent progress on ferroelectric polymer-based nanocomposites for high energy density capacitors: synthesis, dielectric properties, and future aspects. *Chem Rev*. 2016;116:4260-4317.
25. Li Q, Han K, Gadinski MR, Zhang G, Wang Q. High energy and power density capacitors from solution-processed ternary ferroelectric polymer nanocomposites. *Adv Mater*. 2014;26:6244-6249.
26. Zhang G, Fan B, Zhao P, et al. Ferroelectric polymer nanocomposites with complementary nanostructured fillers for electrocaloric cooling with high power density and great efficiency. *ACS Appl Energy Mater*. 2018;1:1344-1354.
27. Kim P, Jones SC, Hotchkiss PJ, et al. Phosphonic acid-modified barium titanate polymer nanocomposites with high permittivity and dielectric strength. *Adv Mater*. 2007;19:1001-1005.
28. Xu W, Yang G, Jin L, et al. High-*k* polymer nanocomposites filled with hyperbranched phthalocyanine-coated $BaTiO_3$ for high-temperature and elevated field applications. *ACS Appl Mater Interfaces*. 2018;10:11233-11241.
29. Li Z, Liu F, Yang G, et al. Enhanced energy storage performance of ferroelectric polymer nanocomposites at relatively low electric fields induced by surface modified $BaTiO_3$ nanofibers. *Compos Sci Technol*. 2018;164:214-221.
30. Zheng MS, Zheng YT, Zha JW, et al. Improved dielectric, tensile and energy storage properties of surface rubberized $BaTiO_3$/polypropylene nanocomposites. *Nano Energy*. 2018;48:144-151.
31. Tang H, Sodano HA. Ultra high energy density nanocomposite capacitors with fast discharge using $Ba_{0.2}Sr_{0.8}TiO_3$ nanowires. *Nano Lett*. 2013;13:1373-1379.
32. Chi Q, Sun J, Zhang C, et al. Enhanced dielectric performance of amorphous calcium copper titanate/polyimide hybrid film. *J Mater Chem C*. 2014;2:172-177.
33. Li H, Ai D, Ren L, et al. Scalable polymer nanocomposites with record high-temperature capacitive performance enabled by rationally designed nanostructured inorganic fillers. *Adv Mater*. 2019;31:1900875.
34. Calebrese C, Hui L, Schadler LS, Nelson JK. A review on the importance of nanocomposite processing to enhance electrical insulation. *IEEE Trans Dielectr Electr Insul*. 2011;18:938-945.
35. Li H, Liu F, Tian H, et al. Synergetic enhancement of mechanical and electrical strength in epoxy/silica nanocomposites via chemically-bonded interface. *Compos Sci Technol*. 2018;167:539-546.

36. Luo S, Yu J, Yu S, et al. Significantly enhanced electrostatic energy storage performance of flexible polymer composites by introducing highly insulating-ferroelectric microhybrids as fillers. *Adv Energy Mater*. 2019;9:1803204.
37. Chen J, Huang X, Sun B, Jiang P. Highly thermally conductive yet electrically insulating polymer/boron nitride nanosheets nanocomposite films for improved thermal management capability. *ACS Nano*. 2018;13:337-345.
38. Li Q, Zhang G, Liu F, et al. Solution-processed ferroelectric terpolymer nanocomposites with high breakdown strength and energy density utilizing boron nitride nanosheets. *Energy Environ Sci*. 2015;8:922-931.
39. Liu F, Li Q, Li Z, et al. Poly(methyl methacrylate)/boron nitride nanocomposites with enhanced energy density as high temperature dielectrics. *Compos Sci Technol*. 2017;142:139-144.
40. Li H, Xie Z, Liu L, et al. High-performance insulation materials from poly(ether imide)/boron nitride nanosheets with enhanced DC breakdown strength and thermal stability. *IEEE Trans Dielectr Electr Insul*. 2019;26:722-729.
41. Azizi A, Gadinski MR, Li Q, et al. High-performance polymers sandwiched with chemical vapor deposited hexagonal boron nitrides as scalable high-temperature dielectric materials. *Adv Mater*. 2017;29:1701864.
42. Huang X, Jiang P. Core–shell structured high-*k* polymer nanocomposites for energy storage and dielectric applications. *Adv Mater*. 2015;27:546-554.
43. Huang Y, Huang X, Schadler LS, He J, Jiang P. Core@ double-shell structured nanocomposites: a route to high dielectric constant and low loss material. *ACS Appl Mater Interfaces*. 2016;8:25496-25507.
44. Luo H, Chen S, Liu L, et al. Core–shell nanostructure design in polymer nanocomposite capacitors for energy storage applications. *ACS Sustain Chem Eng*. 2018;7:3145-3153.
45. Li Z, Liu F, Li H, et al. Largely enhanced energy storage performance of sandwich-structured polymer nanocomposites with synergistic inorganic nanowires. *Ceram Int*. 2019;45:8216-8221.
46. Zhang X, Jiang J, Shen Z, et al. Polymer nanocomposites with ultrahigh energy density and high discharge efficiency by modulating their nanostructures in three dimensions. *Adv Mater*. 2018;30:1707269.
47. Jiang J, Shen Z, Cai X, et al. Polymer nanocomposites with interpenetrating gradient structure exhibiting ultrahigh discharge efficiency and energy density. *Adv Energy Mater*. 2019;9:1803411.
48. Wang Y, Chen J, Li Y, Niu Y, Wang Q, Wang H. Multilayered hierarchical polymer composites for high energy density capacitors. *J Mater Chem A*. 2019;7:965-2980.
49. Wang Y, Wang L, Yuan Q, et al. Ultrahigh energy density and greatly enhanced discharged efficiency of sandwich-structured polymer nanocomposites with optimized spatial organization. *Nano Energy*. 2018;44:364-370.
50. Coleman JN, Lotya M, O'Neill A, et al. Two-dimensional nanosheets produced by liquid exfoliation of layered materials. *Science*. 2011;331:568-571.
51. Niu Y, Wang H. Dielectric nanomaterials for power energy storage: surface modification and characterization. *ACS Appl Nano Mater*. 2019;2:627-642.
52. Pan Z, Yao L, Zhai J, Yao X, Chen H. Interfacial coupling effect in organic/inorganic nanocomposites with high energy density. *Adv Mater*. 2018;30:1705662.
53. Shen ZH, Wang JJ, Lin Y, et al. High-throughput phase-field design of high-energy-density polymer nanocomposites. *Adv Mater*. 2017;30:1704380.

SUPPORTING INFORMATION

Additional supporting information may be found online in the Supporting Information section at the end of this article.

How to cite this article: Li H, Ren L, Ai D, et al. Ternary polymer nanocomposites with concurrently enhanced dielectric constant and breakdown strength for high-temperature electrostatic capacitors. *InfoMat*. 2019;1–12. https://doi.org/10.1002/inf2.12043